

Deep Learning Predicts Prevalent and Incident Parkinson’s Disease From UK Biobank Fundus Imaging

Charlie Tran¹, Kai Shen¹, Kang Liu², and Ruogu Fang^{1,3,4,5,*}

¹Dept. of Electrical and Computer Engineering, University of Florida, Gainesville, FL 32611, USA

²Dept. of Physics, University of Florida, Gainesville, FL, 32661, USA

³J. Crayton Pruitt Family Dept. of Biomedical Engineering, University of Florida, Gainesville, FL 32611, USA

⁴Center for Cognitive Aging and Memory, University of Florida, Gainesville, FL 32611, USA

⁵Dept. of Computer and Information Science and Engineering, University of Florida, Gainesville, FL. 32611, USA

Abstract

Parkinson’s disease is the world’s fastest growing neurological disorder. Research to elucidate the mechanisms of Parkinson’s disease and automate diagnostics would greatly improve the treatment of patients with Parkinson’s disease. Current diagnostic methods are expensive with limited availability. Considering the long progression time of Parkinson’s disease, a desirable screening should be diagnostically accurate even before the onset of symptoms to allow medical intervention. We promote attention for retinal fundus imaging, often termed a window to the brain, as a diagnostic screening modality for Parkinson’s disease. We conducted a systematic evaluation of conventional machine learning and deep learning techniques to classify Parkinson’s disease from UK Biobank fundus imaging. Our results suggest Parkinson’s disease individuals can be differentiated from age and gender matched healthy subjects with 71% accuracy. This accuracy is maintained when predicting either prevalent or incident Parkinson’s disease. Explainability and trustworthiness is enhanced by visual attribution maps of localized biomarkers and quantified metrics of model robustness to data perturbations.

Introduction

Parkinson’s disease (PD) is the world’s fastest-growing neurological disorder. PD is characterized by severe motor control abnormalities and non-motor symptoms. The manifestation of these symptoms is pathologically characterized by the significant loss of dopaminergic neurons in the substantia nigra. An estimated one million individuals in the United States have PD, leading to nearly \$50 billion a year in economic burden.¹ Notably, this financial burden consists not only of direct medical costs but also indirect influences such as necessitated family care and social welfare. The World Health Organization estimates the prevalence of PD has doubled in the last 25 years, while the number of deaths caused by PD increased by over 100% since 2000, largely due to the lack of effective intervention under the rising growth of the elderly population.² Innovations to our understanding of the pathology of PD and the development of early diagnostic systems are desired to address the global concerns arising from PD.

Systematic diagnostic evaluation of PD currently struggles due to the lack of early biomarkers and balance between both specificity and sensitivity.³ Indeed, cardinal motor symptoms fall within the umbrella of Parkinsonism, while non-motor indicators are symptomatic of numerous neurodegenerative diseases. Risk factors such as age, gender, and environmental toxin exposure are not specific to PD. Differential diagnosis frameworks established by the UK’s Parkinson’s Disease Society Brain Bank and the International Parkinson and Movement Disorder Society⁴ are the current standards for evaluation. However, these *checklists* require increasing amounts of exclusion and evidence, including response to dopaminergic therapy (levodopa), and even DaTscan imaging to conclude a definitive PD diagnosis. Moreover, early or atypical PD complicates the observability of cardinal signs, leading to significantly reduced diagnostic accuracy.^{5,6} Thus, current diagnostic indicators lack solid predictive power, straining diagnostic expenses, time, availability, and subjectivity.

The retina provides a routine, inexpensive, and non-invasive modality for studying brain-related pathological processes of neurodegenerative diseases, often referred to as *a window to the brain*.^{7–10} Dopamine plays a complex role in visual pathway processing, justifying visual dysfunction findings in PD individuals.¹¹ Moreover, substantial evidence has revealed large temporal gaps between the onset of PD and observable symptoms, inspiring the retina as a prodromal PD biomarker.¹² Clinical studies have suggested retinal layer thinning and reductions in microvasculature

density in PD patients primarily through optical coherence tomography (OCT).^{13,14} Nonetheless, clinical findings with regards to both retinal degeneration and disease-specific information (disease duration, disease severity, etc.) are not always consistent,^{15,16} demanding further studies to bolster retinal diagnostic power.

Artificial intelligence (AI) algorithms are efficient diagnostic tools through their ability to identify, localize, and quantify pathological features, as evident from their success in diverse retinal disease tasks.^{17,18} Learning retinal biomarkers of PD demands an intricate understanding of structural degeneration of the retinal vasculature, a task unfeasible for even experienced ophthalmologists. To combat this challenge, we propose the usage of AI algorithms to extract the complex relationships existing within the global and local spatial levels of the retina.

We provide one of the first comprehensive artificial intelligence studies of PD classification from fundus imaging. Our key objective is realized by systematically profiling the classification performance across different stages of Parkinson's disease progression, namely incident (consistent with pre-symptomatic and/or prodromal) PD and prevalent PD. Improving upon other related works, we maximize the diagnostic capacity of AI algorithms by neglecting the usage of any external quantitative measures or feature selection methods. Finally, we assess diagnostic consistency and robustness through extensive experimentation of both conventional machine learning and deep learning approaches together with a post-hoc spatial feature attribution analysis. Overall, this work enables future research in the development of efficient diagnostic technology and early disease intervention.

Methods

UK Biobank Participants

The UK Biobank (UKB) is one of the largest biomedical databases, recruiting over 500,000 individuals aged 40-69 years old at baseline throughout assessment centers in the United Kingdom in 2006-2010. The methods by which this data was acquired have been described elsewhere.¹⁹ Diverse patient health records include demographic, genetic, lifestyle, and health information. Comprehensive physical examinations as well as ophthalmic examinations were conducted for further analysis. Health-related events were determined using data linkage to the Health Episode Statistics (HES), Scottish Morbidity Record (SMR01), Patient Episode Database for Wales (PEDW), and death registers.

Parkinson's Disease and Definitions

Parkinson's disease was determined by hospital administration data in the United Kingdom, national death register data, and self-reported data. We consider *prevalent* PD subjects diagnosed prior to baseline assessment and *incident* PD subjects diagnosed following baseline assessment. Prevalent PD subjects were labeled according to hospital admission electronic health records based on the International Classification of Diseases (ICD9, ICD10) codes or self-reports. Incident PD subjects were labeled according to either the ICD codes or the death registry. The earliest recorded diagnostic dates take priority in case of multiple records. If PD was recorded in the death register only (diagnosed post-mortem), the date of death is used for the date of diagnosis. In particular, we acquire our PD labels according to the UKB Field 42030. Further details may be inquired upon from the UKB documentation.²⁰

Ophthalmic Measures

In the UKB eye and vision consortium, the ophthalmic assessment included (1) questionnaires of past ophthalmic and family history, (2) quantitative measures of visual acuity, refractive error, keratometry, and (3) imaging acquisition including spectral domain optical coherence tomography (SD-OCT) of the macula and a disc-macula fundus photograph. In our study, we acquire diagnostic fields of eye problems, visual acuity measured as the logarithm of the minimum angle of resolution (LogMar), and fundus photographs. Fundus photographs were acquired using a Topcon 3D OCT-1000 Mark II system. The system has a 45° field angle, scanning range of 6 mm × 6 mm centered on the fovea, acquisition speed of 18,000 A-scans per second, and 6 μm axial resolution. The details of the eye and vision consortium have been described in other studies.²¹

Study Population and Summary Statistics

A total of 175,824 fundus images from 85,848 subjects were discovered in the UKB (as of 2019 October, UKB). Among this population, we found 585 fundus images from 296 subjects with Parkinson's disease. Manual image quality selection was performed to exclude images according to external guidelines,¹⁷ including artifacts, clarity, and field definition defects. Following manual selection, a total of 123 usable Parkinson's disease images from 84 subjects were found to have met our criteria for inclusion. For each PD image, a healthy control (HC) with no history of PD was matched according to their age and gender to prevent covariate bias. All other fundus images and corresponding subjects were excluded. This constitutes our binary-labeled *overall* dataset of 246 fundus images (123 PD, 123 HC)

from 175 subjects (84 PD, 91 HC). Lastly, we form two subsets of the data corresponding to a *prevalent dataset* of 146 fundus images (73 PD, 73 HC) from 108 subjects (53 PD, 55 HC) and an *incident dataset* of 100 fundus images (50 PD, 50 HC) from 69 subjects (31 PD, 38 HC). The data collection pipeline is summarized in Figure 1.

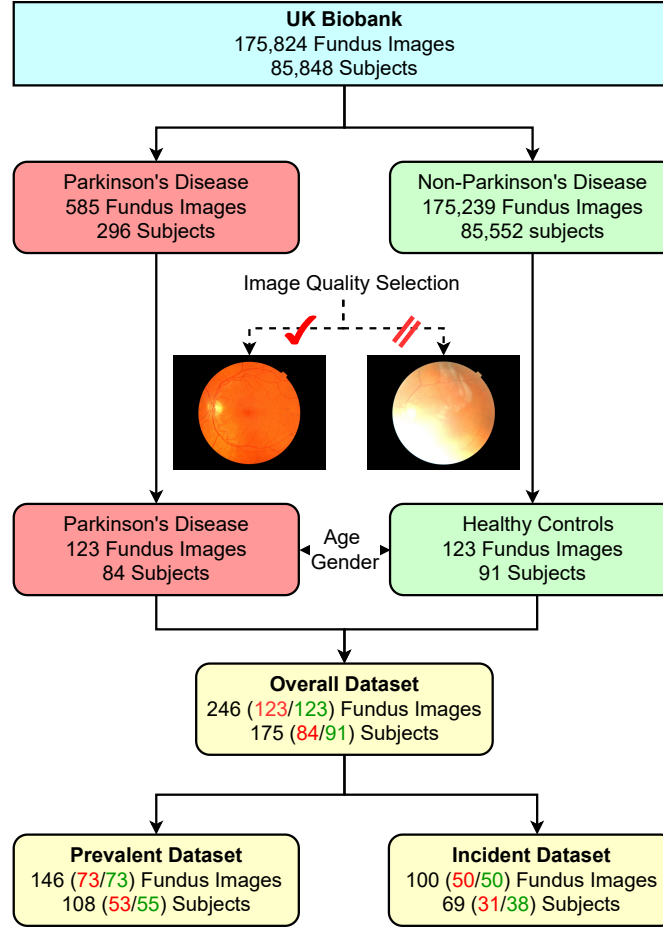


Figure 1. Data Collection pipeline from the UK Biobank. Instances highlighted in red correspond to Parkinson’s disease and instances corresponding to green correspond to healthy controls. Manual quality selection is used to select images of sufficient image quality. In total, we have the *overall* dataset of PD subjects matched with age and gender-matched healthy controls, and two subsets corresponding to *prevalent* and *incident* subjects.

Risk factors of Parkinson’s disease have been extensively studied,^{22–24} including age, gender, ethnicity, Townsend deprivation indices, alcohol consumption, history of obesity-diabetes, history of stroke, and psychotropic medication usage. Moreover, the effects of Parkinson’s Disease have been associated with visual symptoms, from which, we acquire a history of diagnostic eye problems and visual acuity measures. We detail the statistical analyses of subject demographics, visual measures, and covariates of our study population in Table 1.

Artificial Intelligence and Model Training

This study explores both deep learning and conventional machine learning models. Specifically, our deep learning models are convolutional neural networks (CNN) including AlexNet,²⁵ VGG-16,²⁶ GoogleNet,²⁷ Inception-V3,²⁸ and ResNet-50.²⁹ Our conventional machine learning models include Logistic Regression, Elastic Net (regularized with hyperparameters $\lambda_{L_1} = 1, \lambda_{L_2} = 0.5$, where L_1 and L_2 designate the respective norms), and support vector machines (linear and radial basis function kernels).

Each of our models is purposed for binary classification with ground-truth labels of 0 (HC) or 1 (PD). We fine-tune our deep learning models pre-trained on ImageNet using a binary cross-entropy loss, Adam optimizer,³⁰ learning rate of $1e-4$, batch size of 64, and 100 epochs with early-stopping. To increase the diversity of our dataset, we apply spatial rotations, horizontal, and vertical augmentations with a probability of 0.4. All images are resized to $256 \times 256 \times 3$ for computational efficiency. Our deep learning models are initialized with ImageNet classification

Baseline Characteristics	PD Group	HC Group	p-value	Prevalent	Incident	p-value
N	84	91	–	53	31	–
Age, mean (SD), years	61.8 (5.9)	61.6 (6.1)	0.86	61.6 (5.8)	62.2 (6.2)	0.66
Gender, No. (%)			0.99			0.62
Male	49 (58.3)	53 (58.2)		32 (60.4)	17 (54.8)	
Female	35 (41.7)	38 (41.8)		21 (39.6)	14 (45.2)	
Ethnicity, No. (%)			0.20			0.44
White	83 (98.8)	87 (95.6)		52 (98.1)	31 (100)	
Others	1 (1.1)	4 (4.4)		1 (1.9)	0 (0)	
Eye Problems, No. (%)			0.63			0.81
Yes	9 (10.7)	13.0 (14.3)		3 (9.7)	6 (11.3)	
No	75 (89.3)	78 (85.7)		28 (90.3)	47 (88.7)	
Visual Acuity, mean (SD)	0.28 (0.38)	0.15 (0.40)	0.03*	0.28 (0.37)	0.29 (0.41)	0.92
Townsend Index, mean (SD)	-1.49 (2.95)	-1.20 (3.05)	0.54	-1.50 (3.11)	-1.44 (2.68)	0.93
Smoking Status, No. (%)			0.27			0.17
Former/Current	30 (35.7)	41 (45.1)		16 (30.2)	14 (45.2)	
Non-Smoker	54 (64.3)	50 (54.9)		37 (69.8)	17 (54.8)	
Drinking Status, No. (%)			0.63			0.61
Former/Current	80 (95.2)	84 (92.3)		50 (94.3)	30 (97.8)	
Non-Smoker	4 (4.8)	7 (7.7)		3 (5.7)	1 (3.2)	
Obesity-Diabetes, No. (%)			0.93			0.06
Yes	21 (25.0)	21 (23.1)		10 (18.9)	11 (35.5)	
No	63 (75.0)	70 (76.9)		43 (81.1)	20 (64.5)	
History of Stroke, No. (%)			0.27			0.27
Yes	3 (3.6)	8 (8.8)		1 (1.9)	2 (6.5)	
No	81 (96.4)	83 (91.2)		52 (98.1)	29 (93.5)	
Psychotropic Medication, No. (%)			–			–
Yes	0 (0)	0 (0)		0 (0)	0 (0)	
No	84 (100)	91 (100)		53 (100)	31 (100)	

Table 1. Baseline Characteristics of the study populations. P-values conducted on continuous data are computed by the Student’s t-test while categorical (binary) variables are computed by Pearson’s Chi-squared test. * indicates statistically significant ($p < 0.05$).

weights, with the input data normalized to the mean and standard deviation of ImageNet. The input of our conventional machine learning models is standardized to unit variance according to the training set’s mean and standard deviation. We test our models using five-fold stratified cross-validation, wherein each fold contains an equal proportion of subjects per class.

Performance Evaluation

The performance of our PD classifiers is averaged over five randomized repetitions of five-fold stratified cross-validation, for a total of 25 testing evaluations. We consider the area under the receiver operating characteristic curve (AUC), accuracy, positive predictive value (PPV), negative predictive value (NPV), sensitivity (true positive rate), specificity (true negative rate), and the F1-score. We note that accuracy can be viewed as a valid metric justified by our stratified cross-validation and balanced dataset. The holistic evaluation is advantageous to allow a number of views regarding diagnostic performance.

Explainability Evaluation

Qualitative visual explanations for our deep learning model predictions are accomplished by the Guided Propagation³¹ algorithm, allowing an interpretable heat map of significant features. Quantitative explanations are provided by the explanation infidelity (INFD) and explanation sensitivity (SENS) metrics (to be distinguished from the classification performance metric *sensitivity*), where a lower result for both INFD and SENS provides evidence for better-robust models. The explanation infidelity and explanation sensitivity are computed at test-time over 50 perturbations drawn from a probability distribution $\mathcal{N} \sim (0, 0.01^2)$, the definitions of which are shown below, and the details

discussed in the corresponding paper.³²

$$\text{SENS}_{\text{MAX}}(\Phi, \mathbf{f}, \mathbf{x}, r) = \max_{\|\mathbf{y}-\mathbf{x}\| \leq r} \|\Phi(\mathbf{f}, \mathbf{y}) - \Phi(\mathbf{f}, \mathbf{x})\|$$
$$\text{INFD}(\Phi, \mathbf{f}, \mathbf{x}) = \mathbb{E}_{\mathbf{I}} \left[(\mathbf{I}^T \Phi(\mathbf{f}, \mathbf{x}) - (\mathbf{f}(\mathbf{x}) - \mathbf{f}(\mathbf{x} - \mathbf{I})))^2 \right]$$

where Φ is an explanation function (e.g., Guided Backpropagation), \mathbf{f} is a black-box model (e.g., CNN), \mathbf{x} is in the input (e.g., fundus image), r is the input neighborhood radius, and \mathbf{I} is the perturbation, here drawn from the noise distribution $\mathcal{N} \sim (0, 0.01^2)$.

Results

Model Performance in Overall PD Groups

The best deep learning model was AlexNet with an average AUC of 0.78, 71% accuracy, 0.67 PPV, 0.78 NPV, 0.82 sensitivity, 0.60 specificity, and 0.73 F1-score. The best conventional machine learning model was the RBF support vector machine with an optimal AUC of 0.76, 68% accuracy, 0.68 PPV, 0.70 NPV, 0.71 sensitivity, 0.66 specificity, and 0.69 F1-score. The VGG-16 classifier performance closely trails the best AlexNet model, while other deep learning and machine learning models perform significantly worse (Figure 2 and Table S1).

Model Performance in Prevalent PD Groups

The best performing deep learning was the VGG-16 model with an average AUC of 0.79, 71% accuracy, 0.71 PPV, 0.74 NPV, 0.73 sensitivity, 0.69 specificity, and 0.71 F1-score. The performance of the AlexNet architecture is nearly identical. The best performing conventional machine learning model was the RBF SVM with an AUC of 0.79, 74% accuracy, 0.76 PPV, 0.74 NPV, 0.71 sensitivity, 0.77 specificity, and 0.72 F1-score, sharing similar performance with Elastic-Net. In general, the performance of the artificial intelligence models increased when restricting the overall PD dataset onto the set of prevalent subjects. Detailed comparisons can be found in Figure 2 and Table S1.

Model Performance in Incident PD Groups

The best-performing deep learning model was the VGG-16 model with an average AUC of 0.80, 71% accuracy, 0.71 PPV, 0.75 NPV, 0.78 sensitivity, 0.64 specificity, and 0.72 F1-score. The performance of the AlexNet and VGG-16 remains similar while other deep learning models decline with less than 65% accuracy. The best-performing conventional machine learning model was the RBF SVM with an AUC of 0.76, 72% accuracy, 0.73 PPV, 0.76 NPV, 0.75 sensitivity, 0.70 specificity, and 0.72 F1-score. The performance of the RBF SVM remains consistent when compared to our other datasets, while other machine learning models decline significantly with less than 65% accuracy. A summarized completion of the results can be found in Figure 2 and Table S1.

Visualization and Explainability

Qualitative explainability is visualized through guided backpropagation on our deep learning models, revealing the models were able to correctly distinguish subtle features on the retinal vasculature (Figure 3). Explanation robustness was found to be the most stable in the AlexNet architecture according to the explanation infidelity and explanation sensitivity metrics (Figure 4). Notably, the VGG-16 attained similar classification performance to AlexNet but is more vulnerable to data perturbations, possibly owing to the large model parameter complexity. Predictions made by other deep learning architectures including GoogleNet, Inception-V3, and ResNet-50 were largely influenced by data perturbations.

Discussion

This work demonstrates deep neural networks can be trained to detect Parkinson’s disease in retinal fundus images with decent performance. In particular, our model can predict the incidence of Parkinson’s disease even before the onset of symptoms, which is a valuable tool to initiate early disease intervention. Automated deep neural networks show strong promises to assist and complement ophthalmologists in terms of biomarker identification and high-throughput evaluation.

Artificial intelligence evaluation of Parkinson’s disease through the retina has been rarely applied. Hu et al.³³ trained a deep learning model to evaluate the retinal age gap as one predictive marker for incident Parkinson’s Disease using fundus images from the UK Biobank, showcasing statistical significance and predictive AUC of 0.71. Nunes et al.³⁴ used optical coherence tomography data to compute retinal texture markers and trained a deep

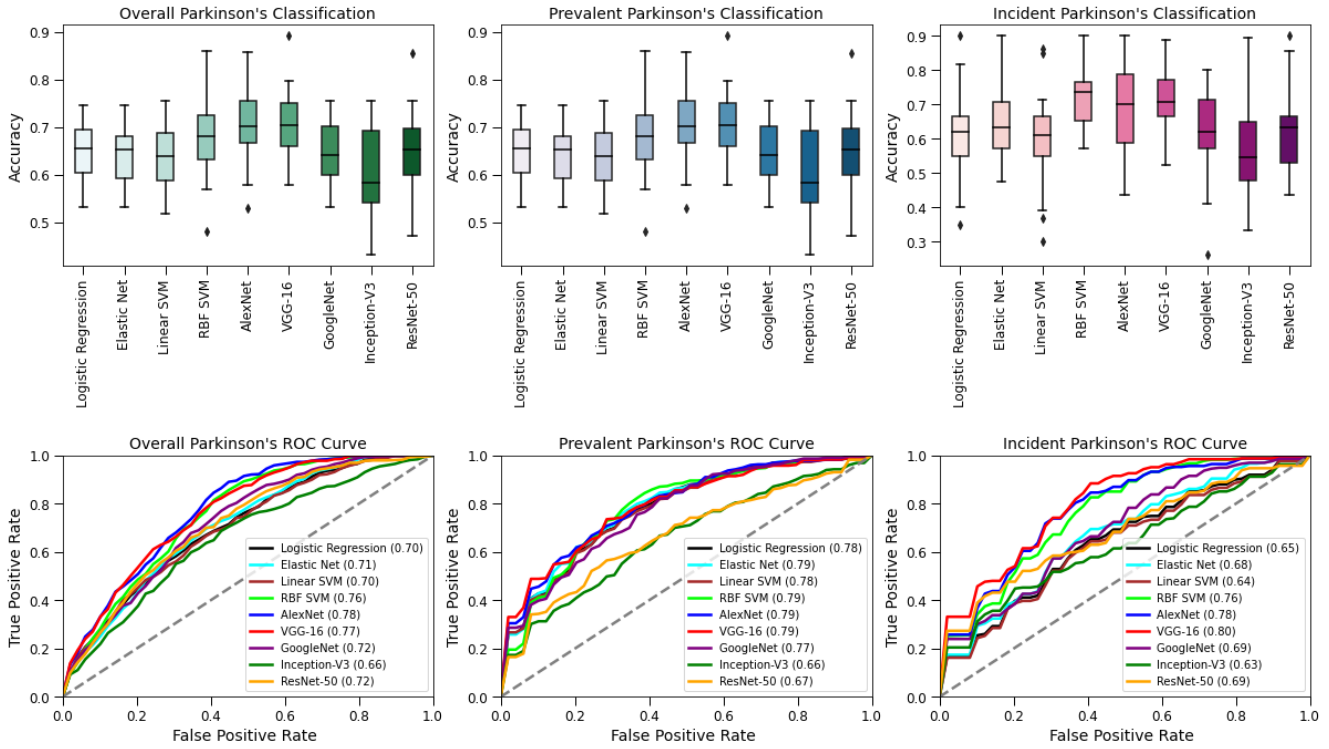


Figure 2. Box-plots and ROC curves of the Parkinson Disease Classification Models. The models are evaluated over five randomized repetitions of the five-fold stratified cross-validation protocol. The AUC scores are enlisted in the legend.

learning model with a median sensitivity of 88.7%, 79.5% and 77.8% with respect to healthy controls, Parkinson’s disease, and Alzheimer’s disease. However, all of these works did not provide a comprehensive comparison of conventional machine learning and deep learning methods on this problem and lacked insights into the explainability of their models. We extend upon these works by treating the entire fundus image as a diagnostic modality, and comprehensively evaluate a broad spectrum of conventional machine learning and deep learning methods, as well as shedding light on the explainability in both image space and on the algorithm level. Our work will lay a solid foundation for future exploration in this direction, and serve as a reference for algorithm selection in terms of both performance and explainability. Related works have been accomplished focusing specifically on Alzheimer’s disease, e.g., Tian et. al³⁵ and Wisely et al.³⁶ but not Parkinson’s disease. Clinical studies in the field have yielded statistical differences in the retinal layers between PD and HC subjects, lacking evidence for diagnostic power. Further work is necessitated in the field of deep learning to build stronger classification performance and understanding of retinal biomarkers. In the future, a multi-modal model utilizing optical coherence tomography, fundus autofluorescence, and/or electronic health records is a considerable direction for Parkinson’s disease analysis.

This study has some limitations. First, the size of our dataset could be enlarged to further capture the wide presentations of Parkinson’s disease. Moreover, the data is derived from the UK population and therefore future studies are needed to evaluate whether these models can generalize to other populations. So far, public datasets containing both Parkinson’s disease subjects and fundus images (as well as patient health records) apart from the UK Biobank are not available, thus new datasets including both retinal images and PD diagnosis in a larger population will be helpful. The next major research question is whether such model explanations are consistent and/or able to guide the grading of ophthalmologists, which is a major goal of clinical translational research. This matter is further complicated as the visual biomarkers for Parkinson’s disease are less well-understood than common eye diseases such as glaucoma. These limitations necessitate future work to ensure the trustworthiness of artificial intelligence models in a clinical setting.

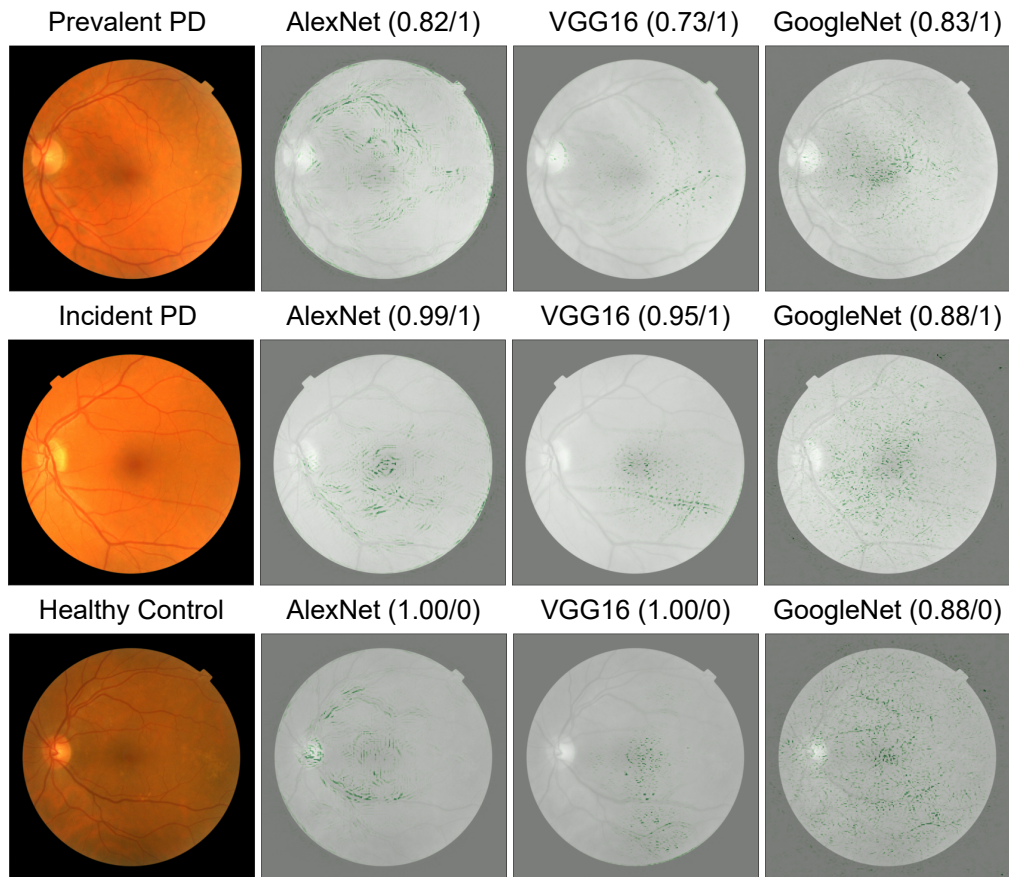


Figure 3. Feature attribution visualizations of random test samples from the top three CNN models (AlexNet, VGG-16, GoogleNet) using the Guided Backpropagation (GBP) algorithm. The predicted probability likelihood and the respective class index (0 HC, 1 PD) is enlisted for each architecture’s prediction. In the left column is the original image (prior to image normalization and resizing). The attribution maps are upsampled to the original image size for visualization.

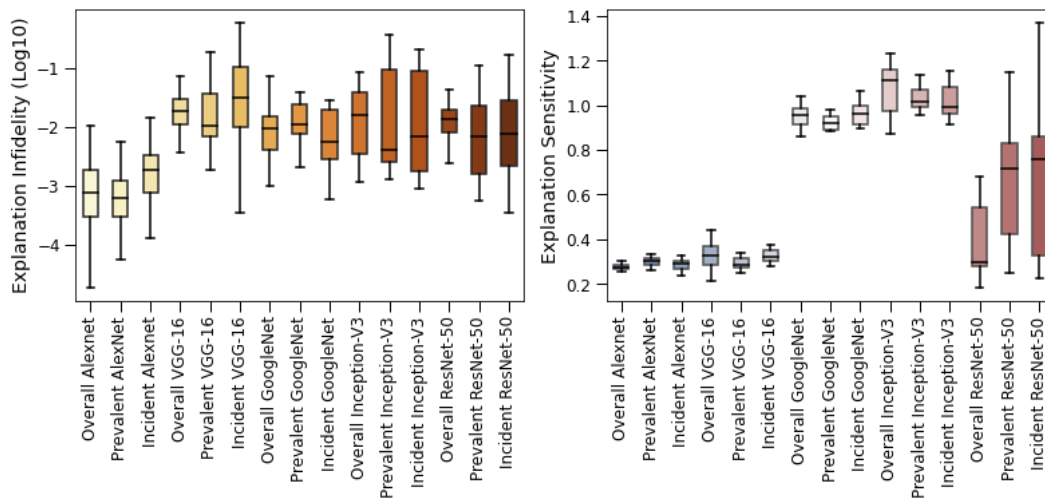


Figure 4. Explanation infidelity and sensitivity comparison among different models. The logarithm of the infidelity score was applied for visualization as a result of the large range of scores.

Conclusion

Deep learning models outperformed conventional machine learning models to accurately predict Parkinson's disease from retinal fundus images. We demonstrate deep learning models can nearly equally diagnose both prevalent and incident PD subjects with robustness to image perturbations, paving the way for early treatment and intervention. Further studies are warranted to verify the consistency of Parkinson's disease evaluation, to enhance our understanding of retinal biomarkers, and to incorporate automated models into clinical settings.

Article Information

Corresponding Author: Ruogu Fang, Ph.D., J. Crayton Pruitt Family Dept. of Biomedical Engineering, University of Florida, Gainesville, FL 32611, USA (ruogu.fang@ufl.edu)

Conflict of Interest Disclosures: The authors declare no competing interests.

Author contributions: Dr. Ruogu Fang and Charlie Tran had full access to all of the data in the study and take responsibility for the integrity of the data and the accuracy of the data analysis.

Study concept and Design: Charlie Tran, Kai Shen, Ruogu Fang.

Acquisition, analysis, or interpretation of data: Charlie Tran, Kai Shen, Kang Liu, Ruogu Fang.

Drafting of the manuscript: Charlie Tran, Kai Shen, Kevin Liu, Ruogu Fang.

Critical revision of the manuscript for important intellectual content: Charlie Tran, Ruogu Fang.

Statistical analysis: Charlie Tran, Kai Shen.

Obtained funding: Ruogu Fang.

Administrative, technical, or material support: Ruogu Fang.

Study Supervision: Ruogu Fang.

Funding/Support: This study was supported by NSF IIS 2123809.

Additional Information: This research has been conducted using the UK Biobank, a publicly accessible database, under Application Number 48388.

Additional Contributions Everett Schwieg, J. Crayton Pruitt Family Department of Biomedical Engineering, University of Florida, provided language editing. None of the contributors received any compensation for this work.

References

1. Yang, W. *et al.* Current and projected future economic burden of parkinson's disease in the U.S. *NPJ Park. Dis.* **6**, DOI: [10.1038/s41531-020-0117-1](https://doi.org/10.1038/s41531-020-0117-1) (2020).
2. World Health Organization. Parkinson disease (2022). Available at <https://www.who.int/news-room/fact-sheets/detail/parkinson-disease>. Accessed electronically on November, 10, 2022.
3. Tolosa, E., Garrido, A., Scholz, S. W. & Poewe, W. Challenges in the diagnosis of parkinson's disease. *The Lancet Neurol.* **20**, 385–397, DOI: [10.1016/s1474-4422\(21\)00030-2](https://doi.org/10.1016/s1474-4422(21)00030-2) (2021).
4. Postuma, R. B. *et al.* MDS clinical diagnostic criteria for parkinson's disease. *Mov. Disord.* **30**, 1591–1601, DOI: [10.1002/mds.26424](https://doi.org/10.1002/mds.26424) (2015).
5. Postuma, R. B. *et al.* Validation of the MDS clinical diagnostic criteria for parkinson's disease. *Mov. Disord.* **33**, 1601–1608, DOI: [10.1002/mds.27362](https://doi.org/10.1002/mds.27362) (2018).
6. Beach, T. G. & Adler, C. H. Importance of low diagnostic accuracy for early parkinson's disease. *Mov. Disord.* **33**, 1551–1554, DOI: [10.1002/mds.27485](https://doi.org/10.1002/mds.27485) (2018).
7. London, A., Benhar, I. & Schwartz, M. The retina as a window to the brain—from eye research to CNS disorders. *Nat. Rev. Neurol.* **9**, 44–53, DOI: [10.1038/nrneurol.2012.227](https://doi.org/10.1038/nrneurol.2012.227) (2012).
8. Gupta, S., Zivadinov, R., Ramanathan, M. & Weinstock-Guttman, B. Optical coherence tomography and neurodegeneration: are eyes the windows to the brain? *Expert. Rev. Neurother.* **16**, 765–775, DOI: [10.1080/14737175.2016.1180978](https://doi.org/10.1080/14737175.2016.1180978) (2016).
9. Archibald, N. K., Clarke, M. P., Mosimann, U. P. & Burn, D. J. The retina in parkinson's disease. *Brain* **132**, 1128–1145, DOI: [10.1093/brain/awp068](https://doi.org/10.1093/brain/awp068) (2009).
10. Devi, S. M., Mahalaxmi, I., Aswathy, N. P., Dhivya, V. & Balachandar, V. Does retina play a role in parkinson's disease? *Acta Neurol. Belg.* **120**, 257–265, DOI: [10.1007/s13760-020-01274-w](https://doi.org/10.1007/s13760-020-01274-w) (2020).
11. Diederich, N. J., Raman, R., Leurgans, S. & Goetz, C. G. Progressive worsening of spatial and chromatic processing deficits in parkinson disease. *Arch. Neurol.* **59**, 1249, DOI: [10.1001/archneur.59.8.1249](https://doi.org/10.1001/archneur.59.8.1249) (2002).
12. Meissner, W. When does parkinson's disease begin? from prodromal disease to motor signs. *Revue Neurol.* **168**, 809–814, DOI: [10.1016/j.neurol.2012.07.004](https://doi.org/10.1016/j.neurol.2012.07.004) (2012).
13. Kwapong, W. R. *et al.* Retinal microvascular impairment in the early stages of parkinson's disease. *Investig. Ophthalmology Vis. Sci.* **59**, 4115, DOI: [10.1167/iovs.17-23230](https://doi.org/10.1167/iovs.17-23230) (2018).
14. Hajee, M. E. *et al.* Inner retinal layer thinning in parkinson disease. *Arch. ophthalmology* **127**, 737–741 (2009).
15. Mailankody, P. *et al.* Optical coherence tomography as a tool to evaluate retinal changes in parkinson's disease. *Park. Relat. Disord.* **21**, 1164–1169, DOI: [10.1016/j.parkreldis.2015.08.002](https://doi.org/10.1016/j.parkreldis.2015.08.002) (2015).
16. Kromer, R. *et al.* Evaluation of retinal vessel morphology in patients with parkinson's disease using optical coherence tomography. *PLOS ONE* **11**, e0161136, DOI: [10.1371/journal.pone.0161136](https://doi.org/10.1371/journal.pone.0161136) (2016).
17. Dai, L. *et al.* A deep learning system for detecting diabetic retinopathy across the disease spectrum. *Nat. Commun.* **12**, DOI: [10.1038/s41467-021-23458-5](https://doi.org/10.1038/s41467-021-23458-5) (2021).
18. Yan, Q. *et al.* Deep-learning-based prediction of late age-related macular degeneration progression. *Nat. Mach. Intell.* **2**, 141–150, DOI: [10.1038/s42256-020-0154-9](https://doi.org/10.1038/s42256-020-0154-9) (2020).
19. Sudlow, C. *et al.* UK biobank: An open access resource for identifying the causes of a wide range of complex diseases of middle and old age. *PLOS Medicine* **12**, e1001779, DOI: [10.1371/journal.pmed.1001779](https://doi.org/10.1371/journal.pmed.1001779) (2015).
20. Bush, K., Rannikmae, K., Wilkinson, T., Schnier, C. & Sudlow, C. Definitions of parkinson's disease and the major causes of parkinsonism, uk biobank phase 1 outcomes adjudication (2018). Available at https://biobank.ndph.ox.ac.uk/showcase/showcase/docs/alg_outcome_pdp.pdf. Accessed electronically on November, 11, 2022.
21. Chua, S. Y. L. *et al.* Cohort profile: design and methods in the eye and vision consortium of UK biobank. *BMJ Open* **9**, e025077, DOI: [10.1136/bmjopen-2018-025077](https://doi.org/10.1136/bmjopen-2018-025077) (2019).
22. Terracciano, A. *et al.* Neuroticism and risk of parkinson's disease: A meta-analysis. *Mov. Disord.* **36**, 1863–1870, DOI: [10.1002/mds.28575](https://doi.org/10.1002/mds.28575) (2021).

23. Kizza, J. *et al.* Cardiovascular risk factors and parkinson's disease in 500, 000 chinese adults. *Annals Clin. Transl. Neurol.* **6**, 624–632, DOI: [10.1002/acn3.732](https://doi.org/10.1002/acn3.732) (2019).
24. Xu, Q. *et al.* Diabetes and risk of parkinson's disease. *Diabetes Care* **34**, 910–915, DOI: [10.2337/dc10-1922](https://doi.org/10.2337/dc10-1922) (2011).
25. Krizhevsky, A., Sutskever, I. & Hinton, G. E. Imagenet classification with deep convolutional neural networks. In Pereira, F., Burges, C., Bottou, L. & Weinberger, K. (eds.) *Advances in Neural Information Processing Systems*, vol. 25 (Curran Associates, Inc., 2012).
26. Simonyan, K. & Zisserman, A. Very deep convolutional networks for large-scale image recognition. *arXiv preprint arXiv:1409.1556* (2014).
27. Szegedy, C. *et al.* Going deeper with convolutions. *CoRR abs/1409.4842* (2014). [1409.4842](https://arxiv.org/abs/1409.4842).
28. Szegedy, C., Vanhoucke, V., Ioffe, S., Shlens, J. & Wojna, Z. Rethinking the inception architecture for computer vision. *CoRR abs/1512.00567* (2015). [1512.00567](https://arxiv.org/abs/1512.00567).
29. He, K., Zhang, X., Ren, S. & Sun, J. Deep residual learning for image recognition. *CoRR abs/1512.03385* (2015). [1512.03385](https://arxiv.org/abs/1512.03385).
30. Kingma, D. P. & Ba, J. Adam: A method for stochastic optimization. *arXiv preprint arXiv:1412.6980* (2014).
31. Selvaraju, R. R. *et al.* Grad-cam: Why did you say that? visual explanations from deep networks via gradient-based localization. *CoRR abs/1610.02391* (2016). [1610.02391](https://arxiv.org/abs/1610.02391).
32. Yeh, C., Hsieh, C., Suggala, A. S., Inouye, D. I. & Ravikumar, P. How sensitive are sensitivity-based explanations? *CoRR abs/1901.09392* (2019). [1901.09392](https://arxiv.org/abs/1901.09392).
33. Hu, W. *et al.* Retinal age gap as a predictive biomarker of future risk of parkinson's disease. *Age Ageing* **51**, DOI: [10.1093/ageing/afac062](https://doi.org/10.1093/ageing/afac062) (2022).
34. Nunes, A. *et al.* Retinal texture biomarkers may help to discriminate between alzheimer's, parkinson's, and healthy controls. *PLOS ONE* **14**, e0218826, DOI: [10.1371/journal.pone.0218826](https://doi.org/10.1371/journal.pone.0218826) (2019).
35. Tian, J. *et al.* Modular machine learning for alzheimer's disease classification from retinal vasculature. *Sci. Reports* **11**, DOI: [10.1038/s41598-020-80312-2](https://doi.org/10.1038/s41598-020-80312-2) (2021).
36. Wisely, C. E. *et al.* Convolutional neural network to identify symptomatic alzheimer's disease using multimodal retinal imaging. *Br. J. Ophthalmol.* **106**, 388–395, DOI: [10.1136/bjophthalmol-2020-317659](https://doi.org/10.1136/bjophthalmol-2020-317659) (2020).

Supplementary

Model	AUC	Accuracy	PPV	NPV	Sensitivity	Specificity	F1	Parameters (M)
Overall (n = 246 fundus images 123 PD, 123 HC)								
Logistic Regression	0.70 (0.68, 0.73)	0.65 (0.62, 0.67)	0.65 (0.62, 0.67)	0.65 (0.62, 0.68)	0.65 (0.60, 0.69)	0.65 (0.61, 0.68)	0.64 (0.61, 0.67)	0.20
Elastic Net	0.71 (0.69, 0.73)	0.64 (0.61, 0.66)	0.64 (0.61, 0.67)	0.64 (0.61, 0.68)	0.64 (0.60, 0.68)	0.64 (0.60, 0.68)	0.63 (0.61, 0.66)	0.20
SVM (Linear)	0.70 (0.68, 0.72)	0.63 (0.60, 0.66)	0.64 (0.61, 0.67)	0.63 (0.60, 0.67)	0.62 (0.57, 0.67)	0.65 (0.61, 0.69)	0.62 (0.59, 0.66)	0.20
SVM (RBF)	0.76 (0.72, 0.79)	0.68 (0.65, 0.72)	0.68 (0.64, 0.72)	0.70 (0.65, 0.75)	0.71 (0.65, 0.76)	0.66 (0.62, 0.71)	0.69 (0.65, 0.72)	0.20
AlexNet	0.78 (0.74, 0.81)	0.71 (0.67, 0.74)	0.67 (0.64, 0.71)	0.78 (0.74, 0.83)	0.82 (0.76, 0.87)	0.60 (0.54, 0.65)	0.73 (0.70, 0.77)	57.0
VGG-16	0.77 (0.73, 0.80)	0.71 (0.68, 0.74)	0.66 (0.73, 0.69)	0.85 (0.81, 0.89)	0.88 (0.84, 0.93)	0.53 (0.46, 0.60)	0.75 (0.73, 0.77)	134.3
GoogleNet	0.72 (0.68, 0.76)	0.65 (0.62, 0.68)	0.67 (0.64, 0.71)	0.64 (0.61, 0.67)	0.60 (0.54, 0.66)	0.70 (0.64, 0.76)	0.62 (0.58, 0.66)	12.0
Inception-V3	0.66 (0.61, 0.71)	0.61 (0.57, 0.65)	0.64 (0.56, 0.72)	0.59 (0.56, 0.63)	0.44 (0.35, 0.54)	0.77 (0.71, 0.84)	0.50 (0.41, 0.58)	21.8
ResNet-50	0.72 (0.68, 0.75)	0.65 (0.61, 0.68)	0.66 (0.62, 0.70)	0.63 (0.57, 0.70)	0.66 (0.58, 0.73)	0.64 (0.55, 0.73)	0.64 (0.58, 0.69)	23.5
Prevalent (n = 146 fundus images 73 PD, 73 HC)								
Logistic Regression	0.78 (0.74, 0.82)	0.70 (0.66, 0.73)	0.70 (0.67, 0.71)	0.71 (0.66, 0.76)	0.70 (0.65, 0.76)	0.70 (0.65, 0.75)	0.70 (0.66, 0.73)	0.20
Elastic Net	0.79 (0.75, 0.83)	0.72 (0.69, 0.75)	0.72 (0.68, 0.76)	0.74 (0.69, 0.78)	0.73 (0.68, 0.79)	0.71 (0.66, 0.76)	0.72 (0.68, 0.76)	0.20
SVM (Linear)	0.78 (0.74, 0.81)	0.69 (0.66, 0.73)	0.70 (0.66, 0.73)	0.70 (0.65, 0.75)	0.69 (0.64, 0.75)	0.69 (0.64, 0.74)	0.69 (0.65, 0.72)	0.20
SVM (RBF)	0.79 (0.75, 0.82)	0.74 (0.70, 0.77)	0.76 (0.71, 0.81)	0.74 (0.69, 0.78)	0.71 (0.65, 0.77)	0.77 (0.71, 0.82)	0.72 (0.68, 0.77)	0.20
AlexNet	0.79 (0.75, 0.84)	0.71 (0.66, 0.75)	0.72 (0.67, 0.77)	0.72 (0.66, 0.77)	0.72 (0.65, 0.79)	0.69 (0.61, 0.76)	0.70 (0.64, 0.76)	57.0
VGG-16	0.79 (0.73, 0.85)	0.71 (0.66, 0.77)	0.71 (0.64, 0.79)	0.74 (0.68, 0.79)	0.73 (0.64, 0.81)	0.69 (0.61, 0.77)	0.71 (0.64, 0.78)	134.3
GoogleNet	0.77 (0.74, 0.81)	0.66 (0.62, 0.70)	0.66 (0.59, 0.73)	0.66 (0.61, 0.70)	0.60 (0.52, 0.68)	0.72 (0.67, 0.77)	0.62 (0.55, 0.69)	12.0
Inception-V3	0.66 (0.59, 0.73)	0.60 (0.54, 0.65)	0.63 (0.52, 0.73)	0.60 (0.54, 0.66)	0.45 (0.34, 0.56)	0.75 (0.66, 0.84)	0.49 (0.39, 0.58)	21.8
ResNet-50	0.67 (0.60, 0.74)	0.60 (0.55, 0.65)	0.59 (0.54, 0.63)	0.61 (0.50, 0.75)	0.84 (0.77, 0.90)	0.38 (0.27, 0.48)	0.68 (0.64, 0.72)	23.5
Incident (n = 100 fundus images 50 PD, 50 HC)								
Logistic Regression	0.65 (0.59, 0.70)	0.61 (0.56, 0.66)	0.62 (0.57, 0.67)	0.61 (0.55, 0.68)	0.62 (0.58, 0.69)	0.60 (0.52, 0.68)	0.61 (0.56, 0.66)	0.20
Elastic-Net	0.68 (0.62, 0.73)	0.64 (0.60, 0.68)	0.64 (0.60, 0.68)	0.66 (0.61, 0.71)	0.68 (0.61, 0.74)	0.61 (0.54, 0.68)	0.65 (0.56, 0.66)	0.20
SVM (Linear)	0.64 (0.58, 0.69)	0.60 (0.55, 0.66)	0.62 (0.56, 0.68)	0.60 (0.54, 0.66)	0.57 (0.50, 0.64)	0.64 (0.55, 0.72)	0.58 (0.53, 0.64)	0.20
SVM (RBF)	0.76 (0.72, 0.81)	0.72 (0.69, 0.76)	0.73 (0.68, 0.78)	0.76 (0.70, 0.81)	0.75 (0.68, 0.82)	0.70 (0.64, 0.77)	0.72 (0.68, 0.77)	0.20
AlexNet	0.78 (0.73, 0.83)	0.69 (0.64, 0.74)	0.69 (0.64, 0.74)	0.71 (0.63, 0.78)	0.71 (0.63, 0.78)	0.67 (0.59, 0.75)	0.69 (0.63, 0.74)	57.0
VGG-16	0.80 (0.76, 0.84)	0.71 (0.68, 0.75)	0.71 (0.66, 0.75)	0.75 (0.66, 0.83)	0.78 (0.71, 0.75)	0.64 (0.55, 0.73)	0.72 (0.69, 0.76)	134.3
GoogleNet	0.69 (0.64, 0.75)	0.61 (0.56, 0.66)	0.63 (0.58, 0.68)	0.61 (0.56, 0.67)	0.57 (0.50, 0.64)	0.65 (0.58, 0.72)	0.59 (0.53, 0.64)	12.0
Inception-V3	0.63 (0.56, 0.70)	0.58 (0.52, 0.64)	0.54 (0.43, 0.65)	0.58 (0.52, 0.65)	0.45 (0.33, 0.57)	0.71 (0.62, 0.80)	0.47 (0.36, 0.58)	21.8
ResNet-50	0.69 (0.61, 0.76)	0.62 (0.58, 0.67)	0.64 (0.55, 0.72)	0.58 (0.46, 0.70)	0.66 (0.54, 0.79)	0.59 (0.45, 0.74)	0.61 (0.53, 0.68)	23.5

Table S1. Classification Results of Parkinson Disease Datasets. For each model, the mean average for each performance metric with their 95% confidence interval is provided over 5 randomized repetitions of 5 fold stratified cross validation. The number of parameters with respect to a $256 \times 256 \times 3$ RGB image input with 2 class outputs is provided for reference and interpretation relative to the model complexity.